Precision Alignment Using a System of Large Rectangular Fresnel Lenses

W. B. Herrmannsfeldt, M. J. Lee, J. J. Spranza, and K. R. Trigger

A system of large rectangular Fresnel lenses has been used in the laser alignment system for the SLAC two-mile accelerator. The alignment system consists of a He–Ne laser light source, a photoelectric detector, and the lenses, one of which is located at each of 297 points which are to be aligned. Each lens has the proper focal length to focus the laser to a point image at the detector. When the alignment at a certain point is to be checked, the image from that lens is scanned by the detector. The image is found to be displaced from its normal position by an amount equal to the product of the position error and the magnification of the lens. The alignment sensitivity is ±0.0025 mm. The targets are enclosed in a 60-cm diam evacuated light pipe to avoid atmospheric disturbances.

Introduction

Accurate optical alignment over very long lengths requires high resolution optics and the elimination of atmospheric disturbance. A system of 297 large, long focal length, rectangular Fresnel lenses is used for the alignment of the Stanford two-mile linear accelerator. The lenses are enclosed in a 60-cm diam vacuum pipe. The system consists of a light source, a detector, and the lenses, one of which is located at each point which is to be aligned.

The tolerance for the alignment of the target points along the accelerator is ±0.25 mm. Conventional optical tooling techniques would require that a very large telescope be pointed at a reference target at the end of the accelerator. The telescope would then have to remain stable until a target at the point to be aligned could be inserted and viewed. The stability requirement would be 0.25 mm/3.0 × 10^6 mm or less than 10^{-7} rad, a virtually impossible tolerance.

The three point method which has been adopted eliminates the high pointing accuracy requirement. Instead, a diverging monochromatic light source is used to illuminate fully the target whose position is to be determined. The target, which functions as a simple converging lens, focuses the light source to an image at the opposite end from the source.

The basic idea of the SLAC alignment system is illustrated in Fig. 1. A straight line is defined between a point source of light L and a detector D. The light source is a helium–neon laser. The detector consists of a mechanical scanning system and a photomultiplier with suitable output equipment capable of resolving a shift of 0.025 mm at any of the 274 support points. The actual sensitivity or least count of the detector is one-tenth of that, or ±0.0025 mm. At each support point, a target T is supported on a remotely actuated hinge. Three additional targets are mounted on monuments, such as the one at M, which are 60-cm diam pillars supported by rock below the accelerator foundation. To check the alignment at a desired point, the target at that point is inserted into the light beam by actuating the hinge mechanism. The target is actually a rectangular Fresnel lens with the correct focal length so that an image of the light source is formed on the plane of the detector. This image is then scanned by the detector in both the vertical and horizontal directions in order to determine the displacement of the target from the predetermined line.

The targets are mounted in a 60-cm diam aluminum pipe (see Fig. 2) which is the basic support girder for the accelerator. The support girder is evacuated to about 0.01 torr to prevent air refraction effects from distorting or deflecting the alignment image. If any adjustments are required, the support girder is moved by means of a pair of vertical screw jacks and a side wall screw jack.

The accelerator proper is mounted about 68 cm above the center of the support girder. Because the optical alignment system is only intended to align the support girder in the horizontal and vertical directions, it is necessary to provide an auxiliary system of levels to prevent azimuthal misalignment of the support girder which, to first order, would have the effect of horizontal misalignment of the accelerator. The azimuthal tolerance is about 1 min of arc. Figure 3 is a

All authors were with Stanford Linear Accelerator Center, Stanford, California 94305, when this work was done; K. R. Trigger is now with Applied Theory, Incorporated, West Los Angeles, California.

Received 21 October 1966.

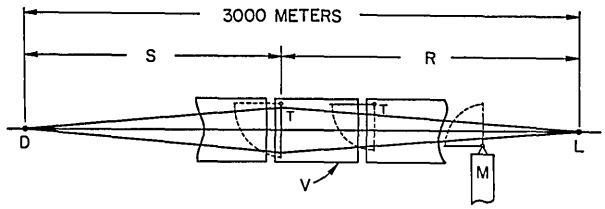

Fig. 1. Schematic illustration of the SLAC alignment system. A typical target T, which is actually a rectangular Fresnel lens, focuses the laser light source L to an image at the detector D. There are 294 alignment targets and three monument targets such as at M, which are attached to deep pillars. V is the 60-cm diam vacuum pipe, 12 m long.

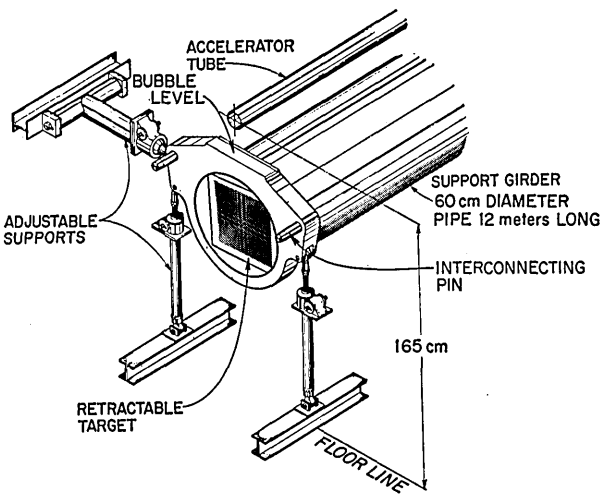

Fig. 2. The mounting arrangement at the target end of each accelerator support girder. The target is shown in the inserted position. When retracted, the target is positioned horizontally along the top of the pipe.

photograph of an installed accelerator segment before the next preceding segment was moved in place.

Over-all Description of the Alignment System

The accelerator is assembled from prefabricated segments which are approximately 12 m long. The standard accelerator segment consists of four 3-m long sections of disk-loaded waveguide mounted on top of a 12-m long section of the 60-cm diam aluminum support girder. At the end of each sector, which consists of eight 12-m long segments, there is a special 3-m long drift section used for steering, focusing, and instrumentation. The standard drift section consists of focusing and steering magnets, beam monitoring devices, and a 16-mm diam collimator mounted on a 3-m long segment of support pipe. There is a total of thirty such sectors, i.e., 240 of the 12-m segments and thirty of the 3-m drift sections, plus three extra segments for the injector and the positron source. As described above, each segment is supported at the input end by a pair of precision screw jacks from the floor and by a third jack from the wall, as shown in Fig. 2. The output end of a segment is attached to the beginning of the next segment by a pair of heavy guide pins which allow for thermal expansion. Both the support girders themselves and the four 3-m long accelerator sections supported on each of them are joined end-to-end by heliarc-welded bellows. A 7.5-cm thick aluminum end flange is welded to the input end of each segment of support pipe. The connecting pins from the three jacks are fastened to the outside of this flange. The target hinge assembly is mounted on the top of the inside surface of the flange. The accelerator sections are supported on adjustable brackets along the support pipe, except that the first support bracket for the section which begins above the flange is pinned in place. The whole design at the input flange is intended to provide the maximum rigidity for the support between the accelerator sections and the alignment target.

The alignment target is mounted on a 40-cm square stainless steel frame. The hinged target support plate is spring-loaded to hold the target firmly against the lower stop when it is inserted in the light beam. A spring-loaded actuator holds the target horizontally against the top of the support girder when it is not being used. In this position the target is hidden behind a square baffle which is mounted in the output end of the adjacent segment of the support girder. One target at a time is to be inserted in the light beam produced by the laser. The target is inserted by operating the bellows actuator which is mounted in an opening on the top of the support girder. The control panel for the target actuator is in the klystron gallery located on the surface directly above the accelerator. Indicator

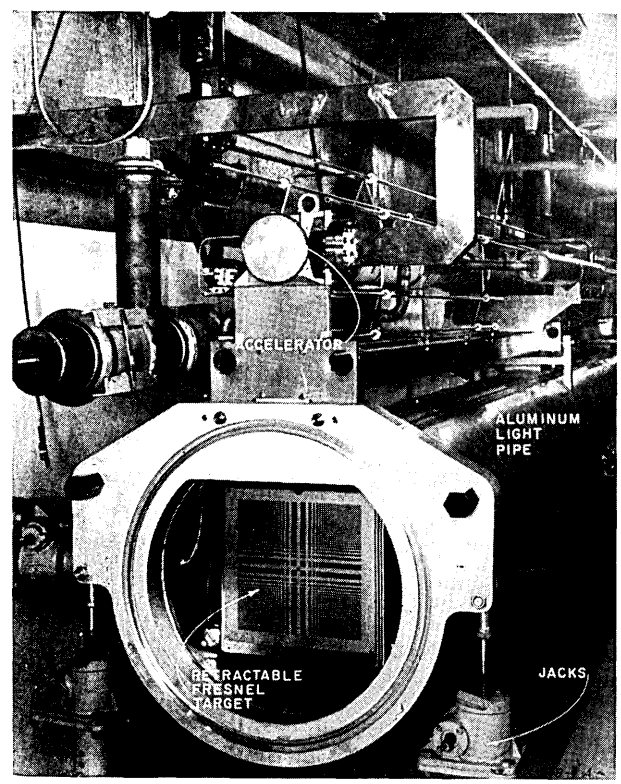

Fig. 3. Photograph of an installed accelerator segment taken prior to installation of the next segment. Adjacent segments are joined by a welded bellows.

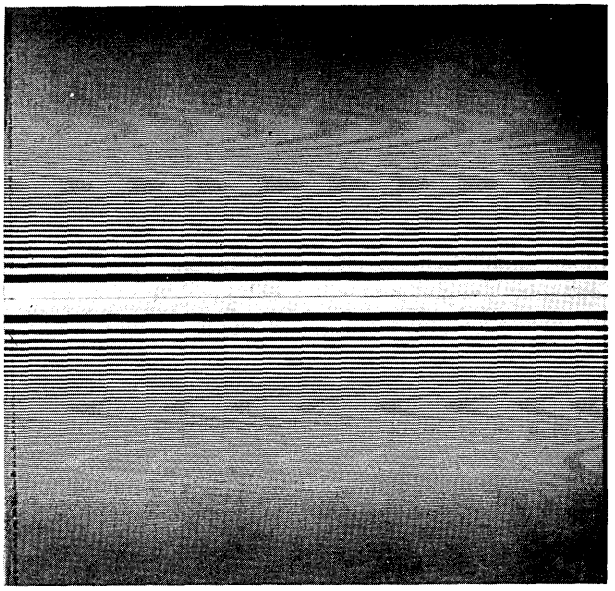

Fig. 4. A one-dimensional Fresnel pattern. The spacing is the same as for a circular Fresnel lens with the same product of focal length and wavelength.

lights wired to microswitches within the support girder show the position of the target to the operator in the klystron gallery. In addition, the operator of the detection equipment at the end of the accelerator has an indicator showing if any target in the entire system is not fully retracted. This indicator assures the operator that only one target at a time is affecting the pattern. The operator also has control switches to permit him to insert remotely one target at each drift section in order to make a quick survey of the key points along the accelerator.

Light Source

The light source for the alignment system is a standard model of a commercial helium–neon gas laser. The targets are designed for the fundamental visible wavelength of 6328 Å. A short focal length lens is mounted on the laser to cause the beam to diverge sufficiently to illuminate fully the closest target which is about 15 m away. This target has a diagonal dimension of about 15 cm, but to insure that the target is evenly illuminated and to reduce further the pointing requirement, the beam is diverged to about twice that diameter. Even with the diverging lens, the intensity of the images as viewed on a ground glass screen is sufficient to be viewed in subdued light. The laser output is from 1.0 mW to 3.0 mW.

Lens Design and Fabrication

The targets are rectangular Fresnel zone plates. The rectangular design is preferred over the classical circular zone plate primarily for reasons of fabrication. It is easier to rule straight lines than circles, and the circular zones would require special spiders for supports. The basic scheme would of course also work with glass lenses. The overwhelming objection to glass is that ordinary glass turns dark in high radiation fields such as are found along the linear accelerator. Also the costs for glass lenses, particularly of radiation resistant material, could be expected to be much greater.

The one-dimensional Fresnel pattern is shown in Fig. 4. The distance from the centerline of the target to the nth slot is

$$X_n = (\lambda rs/2l)^{\frac{1}{2}}(4n)^{\frac{1}{2}}. \quad (1)$$

This is the same expression that is derived for the radius of the $2n$ Fresnel zone in most standard optics texts.[1] In it, λ is the wavelength, r and s are, respectively, the distances from the target to the laser and to the detector, and $l = r + s$. The edges of the nth slot are at

$$X_{ni} = (\lambda rs/2l)^{\frac{1}{2}}(4n + d - 1)^{\frac{1}{2}}$$

and (2)

$$X_{no} = (\lambda rs/2l)^{\frac{1}{2}}(4n + d + 1)^{\frac{1}{2}}.$$

The subscripts i and o denote the inner and outer edges of a slot, respectively. The arbitrary constant d selects the point at which the slot edge will be located in each Fresnel zone. For example, the values 0.0 and 2.0 for d have the effect of making two patterns which are the inverse or negatives of each other.

The targets are formed by chemically milling the array of rectangular holes into a copper sheet which is about 35 cm square and 0.5 mm thick. The following step-by-step manufacturing process is used:

1) Rule the complete one-dimensional pattern on a coated glass plate with an automatic diamond-tipped ruling engine controlled by punched paper tape, generated from computer magnetic tape output.

2) Strip the coating from the area between the edges of the open slots to form the pattern shown in Fig. 4.

3) By a succession of photographic steps, all using

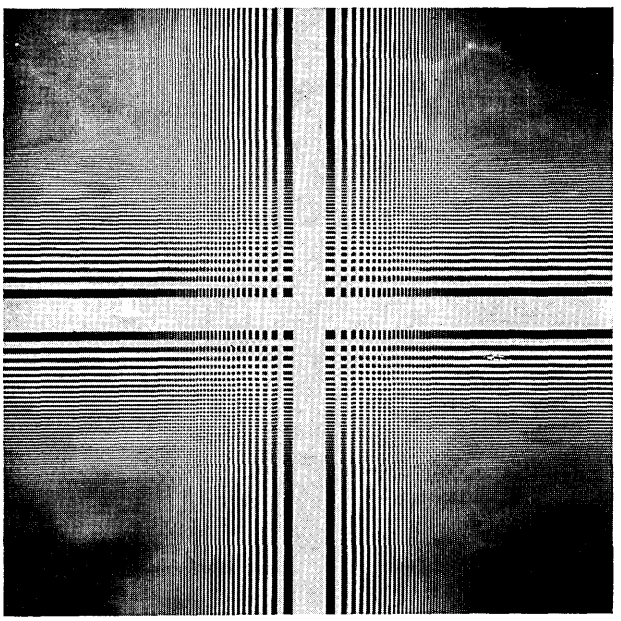

Fig. 5. The crossed pattern of the rectangular Fresnel lens. The actual lenses have open spaces in the dark areas. The opaque center ribbon, 1 cm in width, provides added structural support.

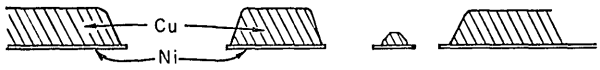

Fig. 6. A cross section of a target showing how the apertures are formed by the 0.05-mm thick nickel plating on 0.5-mm thick copper sheets. When the holes are small and closely spaced, all the copper may be removed.

contact printing, form a master pattern consisting of crossed images of the one-dimensional pattern as shown in Fig. 5.

4) Transfer the master pattern to the copper sheet by applying a light-sensitive coating known as photoresist and by exposing the coated copper to the master pattern. The nature of the photoresist coating is such that, after developing and fixing, it is possible to use a suitable solvent to wash away the coating where the copper has not been exposed. The resulting areas of clean copper may then be used for subsequent plating or etching operations.

5) Electroplate an 0.05-mm thick layer of nickel on the clean copper to form the actual pattern of the target.

6) By chemical milling, remove the unplated copper to form the required pattern of holes as in Fig. 5. The chemical milling process is controlled to retain the copper behind the nickel plating wherever possible. Generally, some copper will remain if the width of the ribbon is greater than the thickness of the copper sheet.

7) Apply a thin flash-coating of nickel for protection to the target which now resembles the cross-section view shown in Fig. 6.

8) Mount the target to the stainless steel frame by match drilling the target and the frame. The frame has a pair of holes which fit over locating pins on the target hinge, thus completing the connection from the target to the accelerator.

Errors in the position of the edges of the apertures can always be divided into symmetric and asymmetric errors. The maximum error that can occur in finding the center of the target is essentially the magnitude of the asymmetric shift of the aperture edges. This conclusion was verified by calculations based on methods which will be used later in this paper. The calculations are detailed in an internal document.[2] The tolerance for the aperture edges is 0.025 mm which is the same as the criteria for the sensitivity of alignment of each target.

Symmetric errors can only affect the intensity and sharpness of the image, never its position. The only important type of symmetric error is that which is proportional to the distance of the edge of the aperture from the center of the target. This error is equivalent to having the wrong focal length for the target as calculated from Eq. (2), where the focal length f is given by $f = rs/l$. The longitudinal distance by which each target can be moved without causing a reduction in alignment sensitivity greater than 10% has been calculated by a digital computer program. In many cases it was found possible to let one target pattern be used in two or more positions without exceeding the 10% limitation. In addition, it is frequently possible to use the same target at an exactly symmetrically located position relative to the center of the accelerator. This is equivalent to exchanging r and s in Eq. (2). As a result, a total of only 121 different patterns is required for the 277 target locations along the accelerator.

Most of the patterns are 30 cm square. However, a limit of 250 slots was set and, as a result, at the ends of the accelerator the targets have 250 lines in less than 30 cm. The smallest of the targets, which is the very last one, is only about 10 cm square. The smallest slot in this last target is about 0.1 mm wide. The target with the longest focal length, which is located at the center of the accelerator, has only forty-six slots in each direction of the 30-cm square.

Detector

The spot or line width of the image at the detection station varies from about 0.1 mm for the last target to about 10.0 mm for the target nearest the light source. Figure 7 shows a photograph of a typical image pattern. The point to be aligned is the spot at the intersection of the crossed lines. The most difficult targets to align are the ones in the center of the accelerator. In this region, line widths are about 4.0 mm. The desired resolution of the alignment system is 0.025 mm. With a 2-to-1 enlargement ratio of a lens in the center of the accelerator, it is necessary to find the center of the spot to within 0.05 mm, or one part in eighty of the line width. This is better than a human operator could be expected to do routinely. Therefore an electromechanical scanning system has been devised which generates the derivative of the spot intensity as a function of detector position in the horizontal or vertical directions. The center of the spot is defined by the point where the derivative is zero. The advantage of

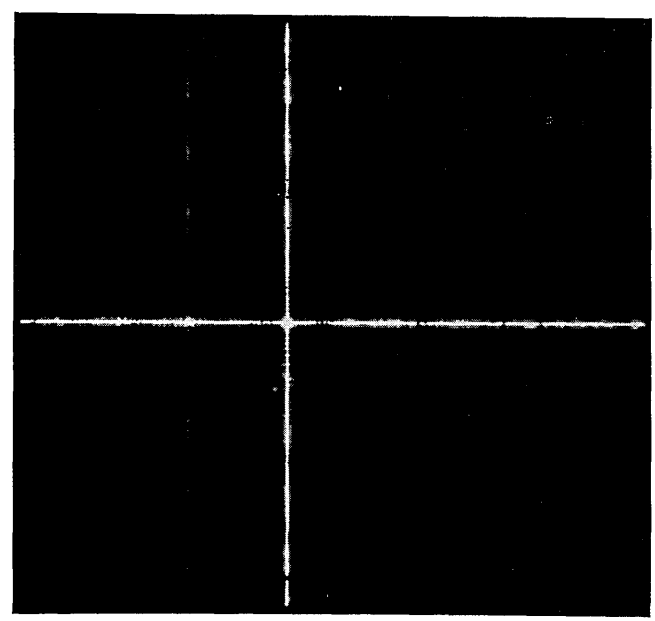

Fig. 7. Photograph of image pattern from a Fresnel lens. The point to be aligned is the spot at the center of the crossed lines. The width of the center spot corresponds to the diffraction limit of the Fresnel lens.

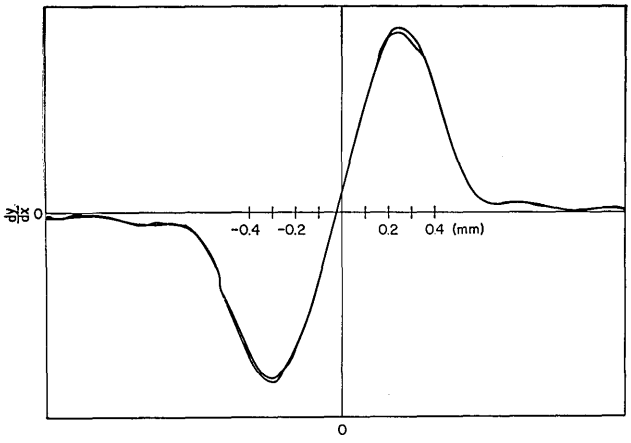

Fig. 8. Plot of the differentiated signal from the photoelectric scanner. The trace was repeated to show the reproducibility of the output.

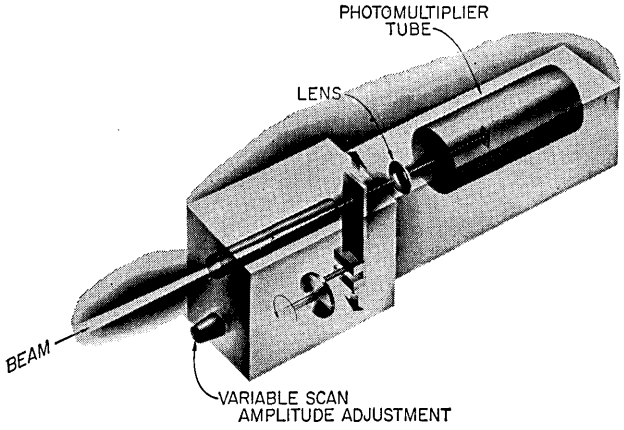

Fig. 9. The variable amplitude scanner and photomultiplier. The scanner may be rotated to sweep either vertically or horizontally.

using this method is that the steep line intersecting the axis gives an unambiguous determination of the image center. Figure 8 shows the actual plot of the differentiated alignment image as obtained from an x–y recorder. The curve was traced twice to establish the reproducibility of the results. Figure 9 shows an artist's cutaway of the detector assembly. The detector can be rotated so that it can scan either horizontally or vertically. A switching mirror system at the detector permits the operator to view the image on a ground glass or to direct it into the detector.

Referring to Fig. 8, the slope of the trace as it crosses the horizontal axis is proportional to the second derivative of the intensity at the peak of the image spot, $(d^2I/d\chi^2)$. When the second derivative of the intensity curve is multiplied by the peak intensity I_o, we obtain a measure of the error signal as a function of displacement of the image. When the square root of this quantity is multiplied by the magnification of the system l/r, resulting product is proportional to the signal obtained by displacing the target, thus giving as a measure of the alignment sensitivity

$$d/d\chi \text{ (output signal)} \propto (l/r)[I_o(d^2I/d\chi^2)]^{\frac{1}{2}}{}_{\chi=o}. \quad (3)$$

Image Pattern

The calculation of the image intensity from a pattern of holes in a target plate involves the use of Fresnel integrals. Both Taylor series approximations of the integrals and digital computer programs have been used for calculating the expected images. The analytical approximation for the rectangular Fresnel lens is presented below.

The intensity of light which has passed through an arbitrary hole pattern at any point P on the image plane is

$$I(P) = |U(P)|^2. \quad (4)$$

For a point source S, the amplitude $U(P)$ is given by the Fresnel-Kirchhoff diffraction integral which, to second order in the variables ξ and η describing the surface, is

$$U(P) = \frac{-Ae^{ikl}}{2l} \iint_{\text{target}} \exp[(i\pi/2)(\mu^2 + \nu^2)]d\mu d\nu, \quad (5)$$

where μ and ν are the normalized distances from the origin P on the target and are given by

$$\mu^2 = (2l/\lambda rs)\xi^2 \text{ and } \nu^2 = (2l/\lambda rs)\eta^2. \quad (6)$$

The wavenumber is $k = 2\pi/\lambda$ and, as in Fig. 10, r and s are the target and image distances, respectively, and $l = r + s$. The point $O(P)$ is the point where the line joining S and P intersects the plane of the target. The source intensity is A^2 units of power.

By taking coordinates ξ and η parallel to the edges of the holes, we can separate the integrals in Eq. (5) and write

$$U(P) = \frac{-Ae^{ikl}}{2l} \int_\mu \exp[i(\pi/2)\mu^2]d\mu \int_\nu \exp[i(\pi/2)\nu^2]d\nu. \quad (7)$$

By substituting Eq. (7) back into Eq. (4), we have

$$I(P) = (A/2l)^2 \{C^2[\mu(P)] + S^2[\mu(P)]\} \times \{C^2[\nu(P)] + S^2[\nu(P)]\} = (A/2l)^2 I_\mu I_\nu. \quad (8)$$

There are a variety of ways to design the target within the mechanical limitations. A simple illustration is to attempt to maximize the C integrals while minimizing

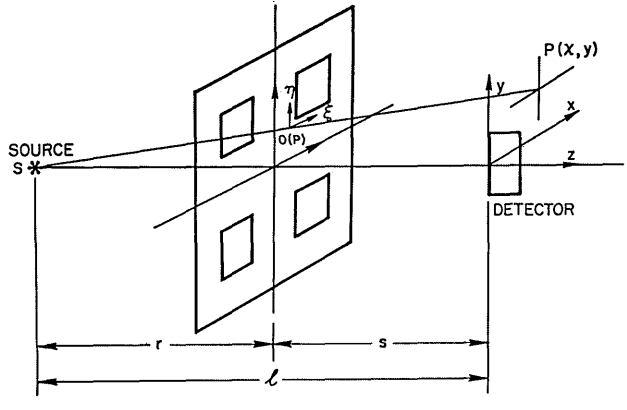

Fig. 10. The coordinate system for calculating the Fresnel integrals. The amplitude $U(P)$ at the detector is found by integrating from the point $O(P)$ on the target.

the S integrals for $P = 0$. If we write

$$C(0) = \int \cos\left(\frac{\pi}{2}\mu^2\right) d\mu \text{ and } S(0) = \int \sin\left(\frac{\pi}{2}\mu^2\right) d\mu, \quad (9)$$

and allow slots at $4n - 1 < \mu^2 < 4n + 1$ and ribbons at $4n + 1 < \mu^2 < 4n + 3$, the $\cos(\pi/2)\ \mu^2$ function will always be positive during intervals of contribution to the integral while the $\sin(\pi/2)\mu^2$ function will oscillate in a manner that causes the integral to be small. The nth slot will then have edges at

$$\xi_+ = (\lambda rs/2l)^{\frac{1}{2}}(4n + 1)^{\frac{1}{2}} \text{ and } \xi_- = (\lambda rs/2l)^{\frac{1}{2}}(4n - 1)^{\frac{1}{2}}. \quad (10)$$

In the case of the targets for the main part of the accelerator, a support strip was required through the middle of each target. This prevented us from including the center or $n = 0$ slot. The best alternative was to make the central ribbon the same width (1 cm) in all targets. Under this circumstance the slot edges as defined by Eq. (10) do not give optimum peak intensity. It is shown in the Appendix that the peak intensity can be maximized by the addition of the constant d under the radical as in Eq. (2), with the value of d determined for each target by the central ribbon width. Since $\lambda f/2$ is different for each target, it is necessary to calculate d from the expression in Eq. (2) for the inner edge of the first slot $X_1{}^2 = (\lambda f/2)(3 + d)$, yielding

$$d = [0.25/(\lambda f/2)] - 3. \quad (11)$$

For this example we will continue to consider the case for $d = 0$, but without the center slot.

Having defined the target pattern as alternating slots and ribbons, we can rewrite the integrals as sums of integrals over the successive slots. Thus we can write

$$C(\epsilon) = \sum_{\substack{n=-N \\ n\neq 0}}^{N} \int_{\mu_{n-}(\epsilon)}^{\mu_{n+}(\epsilon)} \cos\left(\frac{\pi}{2}t^2\right) dt \quad (12)$$

and

$$S(\epsilon) = \sum_{\substack{n=-N \\ n\neq 0}}^{N} \int_{\mu_{n-}(\epsilon)}^{\mu_{n+}(\epsilon)} \sin\left(\frac{\pi}{2}t^2\right) dt, \quad (13)$$

where ϵ is the normalized displacement from P at the point where the line from L to the point of interest on the image plane crosses the target. Thus for the intensity at the peak, the integrals are evaluated for $\epsilon = 0$. By measuring ϵ in the normalized coordinates, as in Eq. (6), the slot edges, which are the limits of integration, become

$$\mu_{n-}(\epsilon) = (4n - 1)^{\frac{1}{2}} - \epsilon \text{ and } \mu_{n+}(\epsilon) = (4n + 1)^{\frac{1}{2}} - \epsilon, \quad \text{for } n > 0$$

and (14)

$$\mu_{n-}(\epsilon) = (4|n| + 1)^{\frac{1}{2}} - \epsilon \text{ and } \mu_{n+}(\epsilon) = -(4|n| - 1)^{\frac{1}{2}} - \epsilon, \text{ for } n < 0.$$

To analyze the intensity of the image near the central maximum we express the one-dimensional intensity of Eq. (8) as a power series in ϵ. Thus we have

$$I_\mu(\epsilon) = C^2(0) + S^2(0) + \epsilon[2C(\partial C/\partial\epsilon) + 2S(\partial S/\partial\epsilon)]_{\epsilon=0} + (\epsilon^2/2)[2(\partial C/\partial\epsilon)^2 + 2C(\partial^2 C/\partial\epsilon^2) + 2(\partial S/\partial\epsilon)^2 + 2S(\partial^2 S/\partial\epsilon^2)]_{\epsilon=0} + \ldots, \quad (15)$$

where

$$\frac{\partial C}{\partial\epsilon} = -\sum_n \left[\cos\left(\frac{\pi}{2}\mu_{n+}{}^2\right) - \cos\left(\frac{\pi}{2}\mu_{n-}{}^2\right)\right],$$

$$\frac{\partial^2 C}{\partial\epsilon^2} = -\pi\sum_n \left[\mu_{n+}\sin\left(\frac{\pi}{2}\mu_{n+}{}^2\right) - \mu_{n-}\sin\left(\frac{\pi}{2}\mu_{n-}{}^2\right)\right],$$

$$\frac{\partial S}{\partial\epsilon} = -\sum_n \left[\sin\left(\frac{\pi}{2}\mu_{n+}{}^2\right) - \sin\left(\frac{\pi}{2}\mu_{n-}{}^2\right)\right], \text{ and}$$

$$\frac{\partial^2 S}{\partial\epsilon^2} = \pi\sum_n \left[\mu_{n+}\cos\left(\frac{\pi}{2}\mu_{n+}{}^2\right) - \mu_{n-}\cos\left(\frac{\pi}{2}\mu_{n-}{}^2\right)\right].$$

For the range of boundaries of interest, good approximations for the integrals are[3]

$$\int_0^\mu \cos\left(\frac{\pi}{2}t^2\right) dt \approx \frac{1}{2} - \frac{1}{\pi\mu}\left[\frac{\cos[(\pi/2)\mu^2]}{\pi\mu^2} - \sin\left(\frac{\pi}{2}\mu^2\right)\right] \quad (16)$$

and

$$\int_0^\mu \sin\left(\frac{\pi}{2}t^2\right) dt \approx \frac{1}{2} - \frac{1}{\pi\mu}\left[\frac{\sin[(\pi/2)\mu^2]}{\pi\mu^2} - \cos\left(\frac{\pi}{2}\mu^2\right)\right]. \quad (17)$$

Using Eq. (16), we have

$$\begin{aligned} C(0) &= \sum_1^N \int_{\mu_{n-}}^{\mu_{n+}} \cos\left(\frac{\pi}{2}t^2\right) dt + \sum_{-1}^{-N} \int_{\mu_{n-}}^{\mu_{n+}} \cos\left(\frac{\pi}{2}t^2\right) dt \\ &= \frac{1}{\pi}\left\{\sum_1^N \left[\frac{\pi}{2} - \frac{\cos(\pi/2)\mu^2}{\pi\mu^3} + \frac{\sin(\pi/2)\mu^2}{\mu}\right]_{(4n-1)^{\frac{1}{2}}}^{(4n+1)^{\frac{1}{2}}} \right. \\ &\quad \left. + \sum_{-1}^{-N} \left[\frac{\pi}{2} - \frac{\cos[(\pi/2)\mu^2]}{\pi\mu^3} + \frac{\sin[(\pi/2)\mu^2]}{\mu}\right]_{-(4|n|-1)^{\frac{1}{2}}}^{-(4|n|+1)^{\frac{1}{2}}}\right\} \\ &= \frac{2}{\pi}\sum_1^N [(4n + 1)^{-\frac{1}{2}} + (4n - 1)^{-\frac{1}{2}}] \approx \frac{2}{\pi}\sum_1^N n^{-\frac{1}{2}}. \end{aligned} \quad (18)$$

Similarly, we can show that

$$\begin{aligned} S(0) &\approx -\frac{2}{\pi^2}\sum_1^N [(4n + 1)^{-3/2} + (4n - 1)^{-3/2}] \\ &\approx \frac{-1}{2\pi^2}\sum_1^N n^{-3/2}. \end{aligned} \quad (19)$$

Except for small values of N, the contribution of $S^2(0)$ to $I_\mu(0)$ is negligible. The sum for $C(0)$ can be approximated by

$$\sum_1^N n^{-\frac{1}{2}} \approx \frac{1}{2}\left[\int_2^{N+1} n^{-\frac{1}{2}} dn + \int_2^{N+1} (n - 1)^{-\frac{1}{2}} dn\right] + 1 = (N + 1)^{\frac{1}{2}} + N^{\frac{1}{2}} - 2^{\frac{1}{2}}. \quad (20)$$

Thus we have

$$C^2(0) = (4/\pi^2)[(N + 1)^{\frac{1}{2}} + N^{\frac{1}{2}} - 2^{\frac{1}{2}}]^2, \quad (21)$$

which agrees with computer calculations of $I(0)$ within 0.25% for $N > 25$.

In completing the expansion to second order for Eq. (15), we find, using the above method,

$$\left.\frac{\partial C}{\partial \epsilon}\right|_0 = \left.\frac{\partial S}{\partial \epsilon}\right|_0 = \left.\frac{\partial^2 S}{\partial \epsilon^2}\right|_0 = 0. \tag{22}$$

The only nonzero term for second order is

$$\frac{\partial^2 C}{\partial \epsilon^2} = -2\pi \sum_1^N [(4n+1)^{\frac{1}{2}} + (4n-1)^{\frac{1}{2}}] \approx -8\pi \sum_1^N n^{\frac{1}{2}}$$

$$\approx -4\pi\left[\int_1^{N+1} n^{\frac{1}{2}} dn + \int_1^{N+1} (n-1)^{\frac{1}{2}} dn\right] \tag{23}$$

$$= -\frac{8\pi}{3}[(N+1)^{3/2} + N^{3/2} - 1].$$

Substituting Eqs. (21), (22), and (23) into Eq. (15) we have

$$I_\mu(\epsilon) \approx (4/\pi^2)[(N+1)^{\frac{1}{2}} + N^{\frac{1}{2}} - 2^{\frac{1}{2}}]^2 \times\left[1 - \epsilon^2 \frac{4\pi^2}{3} \frac{(N+1)^{3/2} + N^{3/2} - 1}{(N+1)^{\frac{1}{2}} + N^{\frac{1}{2}} - 2^{\frac{1}{2}}} + \ldots\right]. \tag{24}$$

For an alignment target formed by superimposing identical patterns at right angles to each other, we can use

$$I_\mu(0) = I_\nu(0). \tag{25}$$

Then, from Eq. (8), with $N \gg 1$, we have

$$I(\epsilon) = (A/l)^2(64N^2/\pi^4)[1 - \epsilon^2(4\pi^2 N/3) + \ldots], \tag{26}$$

which describes the intensity near the peak along one of the axis lines through the center.

Detector Signals

The methods used to analyze the image intensity from the rectangular Fresnel lens will now be extended to study the signal from the detector. The image is scanned in one direction at a time by a linearly oscillating aperture which moves parallel to the direction in which the scanning motion is made. A phase-sensitive detector is used to analyze the signal. To get an analytical conception of the signal amplitude, slope, and line width, we expand the image in a Taylor series.

If $H(x,y)$ describes an aperture located at x and y on the image plane, the power into a photomultiplier tube placed behind the aperture is

$$P(x,y) = \left(\frac{A}{2l}\right)^2 \int_{H(x,y)} I(\xi) I(\eta) d\xi d\eta. \tag{27}$$

As defined in Eq. (6), ξ and η are measured in the target plane. $I(\xi)$ and $I(\eta)$ can be expanded in a Taylor series as

$$I(\xi) = I(0) + \xi I^{(1)} + (\xi^2/2) I^{(2)} + \ldots, \tag{28}$$

where $I^{(n)} = (\partial^n I/\partial \xi^n)_{\xi=0}$. It is convenient to calculate using a rectangular aperture with dimensions $2a$ wide by $2b$ high. Then the integral in Eq. (27) becomes

$$\int_{H(x,y)} I(\xi) I(\eta) d\xi d\eta = \left(\frac{r}{l}\right)^2 \int_{x-a}^{x+a} I(\xi) d\xi \int_{y-b}^{y+b} I(\eta) d\eta, \tag{29}$$

where the r/l factors come from measuring ξ and η at the image plane.

If the scan is made in the x direction right through the peak of the image at $y = 0$, we have

$$\frac{r}{l}\int_{-b}^{b} I(\eta) d\eta = 2I(0)b + \frac{2}{3!} I^{(2)} b^3 + \ldots = G(0) \tag{30}$$

and

$$\frac{r}{l}\int_{x-a}^{x+a} I(\xi) d\xi = 2I(0)a + 1/2[(x+a)^2 - (x-a)^2] I^{(1)} + 1/3![(x+a)^3 - (x-a)^3] I^{(2)} + 1/4![(x+a)^4 - (x-a)^4]\, I^{(3)} + 1/5![(x+a)^5 - (x-a)^5] I^{(4)} + \ldots$$

$$= 2I(0)a + 2xaI^{(1)} + [ax^2 + (a^3/3)] I^{(2)} + (xa/3)(x^2 + a^2) I^{(3)} + 2a/5!(5x^4 + 10x^2a^2 + a^4) + \ldots$$

$$= F(x). \tag{31}$$

The motion of the aperture is described by

$$x = x_0 + d \sin\omega t, \tag{32}$$

where x_0 is the position of the center of oscillation at time t and the amplitude of oscillation is d. From Eq. (32) we have

$$x^2 = x_0^2 + 2x_0 d \sin\omega t + d^2 \sin^2\omega t,$$

$$x^3 = x_0^3 + 3x_0^2 d \sin\omega t + 3x_0 d^2 \sin^2\omega t + d^3 \sin^3\omega t, \text{ and}$$

$$x^4 = x_0^4 + 4x_0^3 d \sin\omega t + 6x_0^2 d^2 \sin^2\omega t + 4x_0 d^3 \sin^3\omega t + d^4 \sin^4\omega t. \tag{33}$$

The output signal can be obtained in terms of the primary oscillating frequency and harmonics by using the following standard trigonometric identities:

$$\sin^2\omega t = \tfrac{1}{2} - \tfrac{1}{2}\cos 2\omega t,$$

$$\sin^3\omega t = \tfrac{3}{4}\sin\omega t - \tfrac{1}{4}\sin 3\omega t,$$

$$\sin^4\omega t = \tfrac{3}{8} - \tfrac{1}{2}\cos 2\omega t + \tfrac{1}{8}\cos 4\omega t. \tag{34}$$

The Fourier analysis can then be made by combining Eqs. (31) through (34) and grouping terms with the same harmonic number. When this is done, the terms with the fundamental frequency are

$$(l/r)F_1(x_0) = 2I^{(1)}ad + 2I^{(2)}adx_0 + I^{(3)}a[x_0^2 d + (a^2 d/3) + (d^3/4)] + \tfrac{1}{3}I^{(4)}a[x_0^3 d + \tfrac{3}{4}x_0 d^3 + x_0 a^2 d] + \ldots. \tag{35}$$

To evaluate Eq. (35) we use the result that [by comparing Eqs. (21) and (24)]

$$I_\mu(\epsilon) \approx \left[\sum_{\substack{n=-N \\ n\neq 0}}^{N} \int_{\mu_n - (\epsilon)}^{\mu_n + (\epsilon)} \cos\left(\frac{\pi}{2}t^2\right) dt\right]^2 = C^2(\epsilon). \tag{36}$$

From the definition in Eq. (6) we have, from Eq. (28),

$$(r/l) I^{(n)} = (2r/\lambda l s)^{n/2} (\partial^n I_\mu/\partial \epsilon^n), \tag{37}$$

where the derivatives are found by successive differentiation of Eq. (36).

The derivatives of the $C(\epsilon)$ integrals follow the pattern used after Eq. (15). If we use the same model target that was assumed in the analysis of the rectangular Fresnel lens, the limits of integration are the same as given by Eq. (14).

Predictably, we find that the odd derivatives are

$$(\partial C/\partial\epsilon)|_{\epsilon=0} = \partial^3 C/\partial\epsilon^3 = 0. \quad (38)$$

For the even derivatives $C(0)$ and $\partial^2 C/\partial\epsilon^2|_{\epsilon=0}$ are given by Eqs. (21) and (23), respectively. Continuing to the fourth derivative from Eq. (15), we obtain,

$$\partial^4 C/\partial\epsilon^4 = (32\pi^3/5)[(N+1)^{5/2} + N^{5/2} - 1]. \quad (39)$$

Combining Eqs. (35) through (39), we find the coefficient of the fundamental frequency is

$$F_1(x_0) \approx -(2r/\lambda ls)(2adx_0)(128N^2/3)$$
$$[1 - (2r/\lambda ls)(x_0^2 + {}^3/_4\, d^2 + a^2)(16\pi^2 N/15) + \ldots]. \quad (40)$$

The width of the image can be defined as the distance between maximum and minimum of $F_1(x_0)$. As such, it is approximately the distance between the positive and negative peaks in Fig. 8 and is about equal to the full width at half maximum. If we assume a and d are small compared to the distance to the maximum or minimum x_m, we have $1 - (16\pi^2/5)\, N x_m^2\, (2r/\lambda ls) = 0$, by setting $[dF_1(x_0)/dx_0] = 0$. From this we find

$$x_m = \pm[(16\pi^2/5)N(2r/\lambda ls)]^{-\frac{1}{2}}. \quad (41)$$

Thus the line width, $x_{\max} - x_{\min}$, is proportional to $(Nr/s)^{-\frac{1}{2}}$.

In practice the light pipe is a constant diameter, thus limiting the targets to a fixed maximum width. If we let $\mu^2 = 4N$ in Eq. (6), ξ would equal the half width of a target so that the effective width of a target is

$$D = (8N\lambda rs/l)^{\frac{1}{2}}. \quad (42)$$

Combining Eqs. (41) and (42), the width of the image is found to be

$$w \approx (5)^{\frac{1}{2}}(\lambda s/\pi D), \quad (43)$$

which, in the middle of the accelerator, is 4.5 mm. Equation (43) is strikingly close to the standard expression for resolution of a lens, $\lambda s/D$.

The detection sensitivity is equal to the derivative of the first harmonic coefficient at $x_0 = 0$. Combining Eqs. (27) and (30) and differentiating, we have $(dP_1/dx_0)|_{x_0=0} \approx (A/2l)^2\, G(0)(dF_1/dx_0)|_{x_0=0}$, which, when we substitute from Eqs. (30) and (40) is

$$(dP_1/dx_0)|_{x_0=0} \approx -(A/2l)^2[(16N/\pi^2)2b](2r/\lambda ls)[(256N^2/3)ad]. \quad (44)$$

If we let the dimensions of the aperture be proportional to the image width such that $b = 2a = fw$, where f is a constant of proportionality, Eq. (44) reduces to

$$(dP_1/dx_0)'_{x_0=0} \approx -17(A/2l)^2 N^2 f^2 d. \quad (45)$$

With a laser source that emits 1 mW into a solid angle of $4\pi \times 10^{-4}$ sr, $(A/2l)^2 \approx 2 \times 10^{-12}$ W/cm^2 for $l \approx 3 \times 10^5$ cm. If we assume the sweep amplitude d of the scanner is equal to $w/2$, we find $|dP_1/dx| \approx 1.7 \times 10^{-11} N^2 f^2 w$ W/cm.

In the center of the accelerator the targets only have 46 lines, or $N = 23$. If we let $f = 1/10$, $|dP_1/dx| \approx 4 \times 10^{-11}$ W/cm. However, since the image from the center target moves twice as far as the target, the alignment sensitivity is

$$|dP_1/d\xi| = (l/r)|dP_1/dx|, \quad (46)$$

which for the center target is about 8×10^{-11} W/cm. To detect a shift of 0.025 mm in the target requires a differentiation of

$$|dP_1/d\xi|\Delta\xi = (8 \times 10^{-11}) \times (0.25 \times 10^{-2})\text{W}, \quad (47)$$

or 2×10^{-13} W for the middle target. The peak intensity, which is the energy striking the photomultiplier at the center of the image, is, from Eqs. (26) and (30),

$$I(0) = (A/2l)^2(256N^2/\pi^4)(2b)(2a)$$
$$= (A/2l)^2\,(512N^2/\pi^4)f^2w^2\ \text{W}. \quad (48)$$

At the center of the accelerator this is about 8.5×10^{-12} W.

Baffles

A baffle plate with a square opening has been mounted in the light pipe at each target position. The dimensions of the hole in each baffle are determined by the criteria that no light may get around a lens when it is inserted and that no direct rays from the laser may hit the inside surface of the pipe.

The combined diffraction pattern from all the baffles is very complex. It is actually such a diffraction pattern, not a spherical wave, which illuminates a lens. The alignment errors resulting from the baffles were calculated in Ref. 2. The method used was to estimate the alignment error as a function of the asymmetry of the diffraction pattern from the baffles. The conclusion is that for any reasonable shift of the baffle, the resulting alignment error is negligible.

Vacuum Requirements

The 60-cm light pipe must be partially evacuated to reduce refractive effects of the residual gas to below the alignment tolerance. Some care was taken during construction to avoid the introduction of heavy solvents or other chemicals with high indices of refraction, so that dry air will be assumed for the following calculations. A large oil diffusion pump with a refrigerated baffle is located at one end of the pipe which has a volume of nearly 10^6 liters. The pumping system has proven capable of reducing the pressure to $\sim 10^{-2}$ torr overnight. At this pressure the system becomes conduction limited.

To calculate the effects of the residual gas we assume that the index of refraction has the form

$$n(y) = n_0(1 - \epsilon y), \quad (49)$$

where $n(y)$ is the index of refraction as a function of the vertical position y, and $n_0\epsilon$ is the gradient of n in the

vertical direction. The vector form of the differential equation of a light ray is[4]

$$(d/ds)[n(d\mathbf{r}/ds)] = \text{grad}n \tag{50}$$

where x is the distance along the ray and $\mathbf{r} = \mathbf{i}x + \mathbf{j}y$, where $\mathbf{i}$ and $\mathbf{j}$ are unit vectors. If we measure x along the axis of the light pipe, then $s = x$ to a very good approximation. Substituting Eq. (49) on the right side of Eq. (50) we have

$$(d/dx)n[\mathbf{i} + \mathbf{j}(dy/dx)] = -\mathbf{j}\epsilon n_0, \tag{51}$$

so that

$$(d/dx)[n(dy/dx)] \approx -\epsilon n_0. \tag{52}$$

If ϵ is small, by integrating Eq. (52) we find

$$y \approx -(\epsilon x^2/2) + Cx + C'. \tag{53}$$

If we study a ray which starts on the axis and parallel to it, both constants of integration are zero and we find

$$y = -(\epsilon x^2/2), \tag{54}$$

which gives the displacement of a light ray due to a gradient of the index of refraction in the light pipe. For the accelerator, the worst case is the middle target so that x is about 1500 m. For an error of 0.025 mm, which is the usual tolerance, we find a value of $\epsilon \approx 2 \times 10^{-13}$/cm.

To determine the gradient of the index of refraction we start with the Lorentz-Lorenz formula in the form[5]

$$A = (RT/p)(n^2 - 1)/3, \tag{55}$$

in which A is the molar refractivity, R is the gas constant, T is temperature, and P is pressure. Because n is very nearly unity we can rewrite Eq. (55) as

$$n - 1 = [3Ap/RT(n + 1)] \approx (3A/2R)(p/T) \tag{56}$$

to obtain the temperature and pressure dependence of $n - 1$. For dry air at standard temperature and pressure we have $n - 1 = 3 \times 10^{-4}$. Thus, at any other temperature T and pressure p, we have

$$n - 1 = 3 \times 10^{-4}(300°\text{K}/760 \text{ torr})(p/T) = 1.2 \times 10^{-4}(p/T), \tag{57}$$

where p and T are measured in torrs and °K, respectively.

To calculate the gradient of the index of refraction due to vertical temperature and pressure gradients we first let

$$p = p_0 + p'y \tag{58}$$

and

$$T = T_0 + T'y, \tag{59}$$

where p' and T' are the derivatives of pressure and temperature with respect to the coordinate y.

By substituting Eqs. (58) and (59) into Eq. (57) and expanding to terms of first order in y, we have

$$n - 1 = 1.2 \times 10^{-4}[(p_0/T_0) + (p'y/T_0) - (p_0T'y/T_0^2) + \ldots]. \tag{60}$$

By comparing terms in Eq. (60) with Eq. (49) we have

$$n_0\epsilon = 1.2 \times 10^{-4}[(p_0T'/T_0^2) - (p'/T_0)]. \tag{61}$$

At 10^{-2} torr, $p' = -1.1 \times 10^{-8}$ torr/cm. The pressure term then becomes $\epsilon_p \approx 4 \times 10^{-15}$/cm which is 1/50th of the tolerance we derived above and is negligible. The temperature gradient from top to bottom of the light pipe is not well known. Differences of about 0.1°C have been measured. If we solve Eq. (61) for T', using the calculated tolerance for $n_0\epsilon$ we have

$$T' = \frac{n_0\epsilon T_0^2}{1.2 \times 10^{-4}P_0} = \frac{2 \times 10^{-13} \times 300^2}{1.2 \times 10^{-4} \times 10^{-2}} \approx 0.015°\text{C/cm}, \tag{62}$$

which means that about 1°C differential is allowed from top to bottom of the 60-cm diam light pipe. It is notable that the temperature term is the term that limits the maximum pressure that we can permit and still stay within the tolerance for alignment.

Operating Results

The theoretical predictions of image size and detector sensitivity have largely been confirmed by experiment. The dimensions of the image patterns agree with the predictions of Eq. (43) except in the case of the targets nearest the laser. For the target closest to the laser it appears that the assumption of a point source is invalid. The image from that target is about 2 cm in diameter instead of the 1 cm calculated assuming a point light source. The magnification for this position is about 200 to 1 meaning that the center only needs to be found to within ±5.0 mm to yield the required accuracy of locating the target. Actually, the sensitivity of determining the position of any target with the photoelectric scanner is ±0.0025 mm, which is the least count of the shaft encoder on the traverse system. The optimum aperture dimensions and scanning amplitudes which were calculated are only partially adhered to in practice. The scanning amplitude is adjusted according to the image width. However, all operation is with a round aperture of 0.1-mm diam. The photomultiplier has a sufficiently sensitive cathode that even this small aperture is enough to give a very adequate signal.

Information about long term stability is obtained by referring to four monuments which are located along the accelerator. Three of the monuments have targets just like the accelerator targets but independent of the accelerator. The fourth monument is used as the base for the detector. Alignment data taken at any time can be calculated with reference to the straight line determined by any two points along the accelerator. Whenever a pair of the monuments is chosen for this purpose, the results give the total shift since the initial alignment.

For the period of operation since April 1966, an alignment check showed some areas had settled by up to 2.5 mm. The results of this survey are shown in Figs. 11 and 12. The largest settlements occurred in areas constructed over filled ground. The correspondence with settlement and fill is quite striking. The implication is that those parts of the accelerator which were built

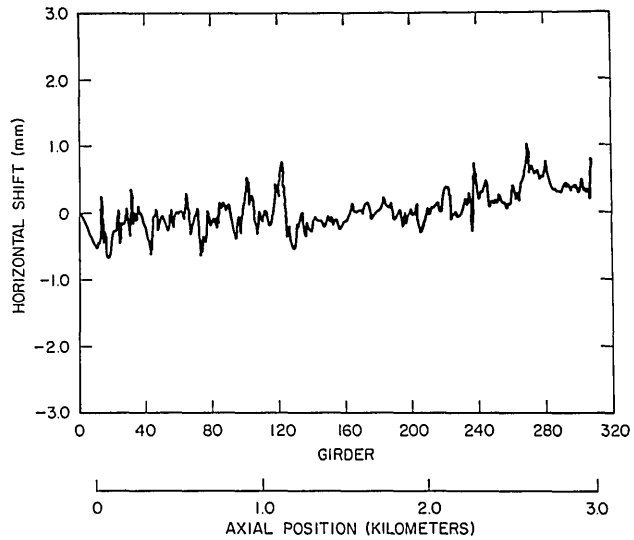

Fig. 11. Horizontal shift from April 1966 to January 1967. The abscissa scale is measured from the west end of the accelerator. The displacements shown are cumulative totals.

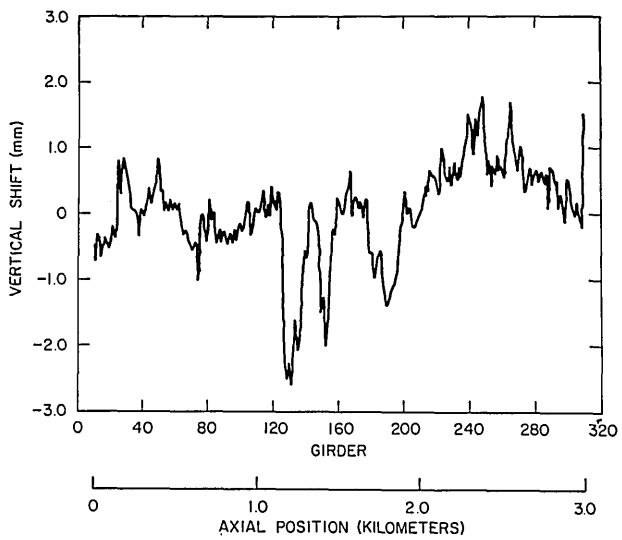

Fig. 12. Vertical shift from April 1966 to January 1967. Normally the accelerator is realigned before the required adjustment can exceed 1 mm.

directly on subsurface rock would be quite stable. Fortunately the more critical areas of the beam switchyard and the end stations are all built directly on the underlying sandstone.

The proximity of the San Andreas fault is often referred to. The fault lies about a kilometer to the west of the accelerator and runs normal to the accelerator. It is too early to tell what effect the presence of the fault may have on the accelerator. There were several very light earth temblors in Northern California in the past few months. No one in the accelerator housing has reported feeling them, however, and beam operation has not been effected. We have not been able to ascribe any motion to the seismic phenomena.

We wish to express our appreciation to SLAC's director, W. K. H. Panofsky. His active participation in developing the concepts of the Fresnel lens system was vital to the success of the program.

The work was supported by the U.S.AEC.

Appendix

For a target pattern having alternate slots and ribbons, the integrals in Eq. (9) can be written as sums of integrals over the slots. We consider two-dimensional vectors

$$\mathbf{V}_n = [C_n(0), S_n(0)]$$

with

$$C_n(0) = \int_{\mu_{n-}}^{\mu_{n+}} \cos\left(\frac{\pi}{2}t^2\right) dt$$

and

$$S_n(0) = \int_{\mu_{n-}}^{\mu_{n+}} \sin\left(\frac{\pi}{2}t^2\right) dt.$$

In terms of these vectors the peak intensity is given by $I(0) = (A/2l)^2 I_\mu I_\nu$, where

$$I_\mu = |\mathbf{V}|^2 = \left|\sum_n \mathbf{V}_n\right|^2$$

and a similar expression for I_ν. Thus, in order to optimize the peak intensity, we must require that the length of the vector V be maximized.

A procedure for maximizing |V| will be illustrated graphically. On a plot of the Cornu spiral we start from a point μ_{1-}, which corresponds to a given central ribbon width of a target, and draw a straight line through the end point of the spiral E as in Fig. 13. The points of intersection of the line with the spiral consti-

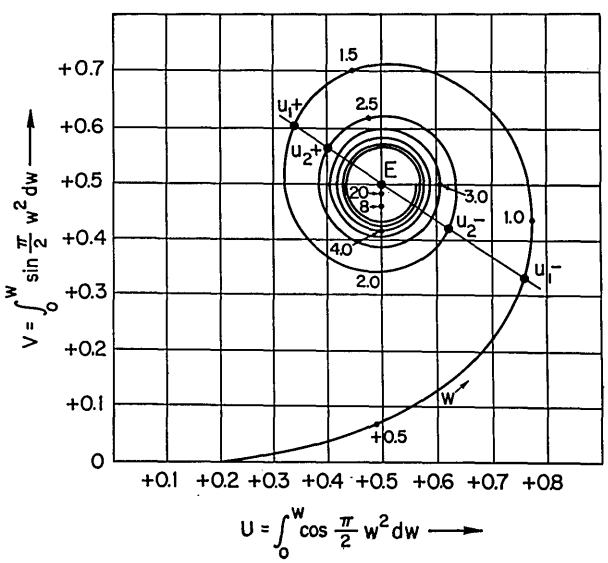

Fig. 13. Cornu spiral used to show graphic method of determining the optimum target design. The point μ_1- corresponds to the edge of the central ribbon. Subsequent slot edges correspond to the intersections of successive spirals with the line joining E and μ_1-.

tute a set of μ_{n+} and μ_{n-} which maximizes $|\mathbf{V}|$. It can be seen that each of the vectors $\mathbf{V}_n$ has an optimum length and all vectors lie along the same direction.

It will be shown analytically that the values of μ_{n+} and μ_{n-} are approximately given by $\mu_{n\pm} = (4n - d + 1)^{\frac{1}{2}}$ with $d = 3 - \mu^2{}_{1-}$, where $\mu_{1-}{}^2 = lw^2/2\lambda rs$ in which w is the width of the central ribbon.

It suffices to show that the slopes of the lines joining $\mu_{n\pm}$ and E are independent on n.

From Eqs. (16) and (17), we find for the slopes of the lines joining $\mu_{n\pm}$ and E

$$M_{\pm}(d) = \frac{\{\sin[(\pi/2)\mu^2{}_{n\pm}]/\pi\mu^2{}_{n\pm}\} - \cos[(\pi/2)\mu^2{}_{n\pm}]}{\{\cos[(\pi/2)\mu^2{}_{n\pm}]/\pi\mu^2{}_{n\pm}\} - \sin[(\pi/2)\mu^2{}_{n\pm}]},$$

from which

$$M_{\pm}(d) = \frac{\sin[(\pi/2)(d \pm 1) - \phi]}{\cos[(\pi/2)(d \pm 1) + \phi]},$$

where $\phi = \tan^{-1} \pi\mu^2{}_{n\pm}$. Since $d < 3$, $\pi\mu^2{}_{n\pm} > 12$ for $n \geq 2$, so that $\phi \approx \pi/2$. Hence,

$$M_{\pm}(d) = \sin(\pi d/2)/\cos(\pi d/2),$$

which being independent of n, proves that the choice of edges is optimized.

References

1. F. Jenkins, and H. White, *Fundamentals of Optics* (McGraw-Hill Book Co., Inc., New York, 1957), 3rd ed.
2. K. R. Trigger, "Approximate solutions of images using Fresnel zone plates," SLAC Internal Report, Stanford Linear Accelerator Center, Stanford University, Stanford, California (1964).
3. M. Born and E. Wolf, *Principles of Optics* (Macmillan Co., New York, 1964), pp. 427–434.
4. Ref. 3, p. 122.
5. Ref. 3, p. 88.

Applied Optics — Optical Activities in Industry

reported by FRANK COOKE, 66 Summer Street, North Brookfield, Mass.
Mr. Cooke welcomes news and comments for this column which should be sent to him at the above address

This month this column reflects another activity in the German optical industry; see the February issue this year for the first part of the feature on Optics in Germany.

Breithaupt Digigon Digital Theodolite

The progress of automatic control in many fields of engineering requires the application of new measuring methods to geodesy. In cooperation with the Geodetic Institute of the Bonn University, F. W. Breithaupt und Sohn developed a digital theodolite that registers the angle values automatically by means of a bidirectional counter (Fig. 1). These angle values are supplied in proper form for subsequent automatic treatment without recomputation. The observer can, at any time, check his measurements, the results of which are shown as clearly visible numbers on the counter.

Dr. Ing. Zetsche suggested incorporating photoelectronic angle transducers in a theodolite in order to eliminate, by the automatic recording of angle values, reading errors and mistakes in manual entries. The Leitz photoelectronic angle transducer incorporated in the Breithaupt digital theodolite is provided with a radial grid disk with 5000 divisions. The rotary motion of the disk, which is connected to the alidade, is transformed into periodic light fluctuations. In order to eliminate remaining eccentricity errors, a portion of the radial grid is electrically illuminated, and a same-size image of the grid division is formed on the diametrically opposite part of the grid. Owing to the fact that the image forming rays are deflected by an even number of reflecting surfaces, this image moves in the opposite direction to the movement of the radial grid disk. The contrarotation of

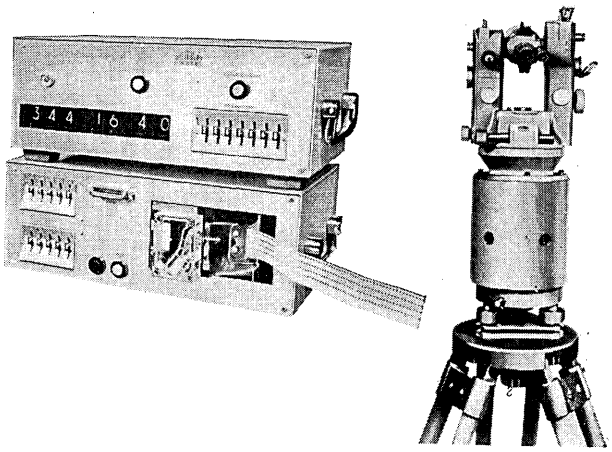

Fig. 1. The Breithaupt digital theodolite with photoelectronic read-out of the circle and bidirectional counter.

grid division and grid image doubles the number of the light periods compared with that of the division periods. Thus 10,000 periods are formed per rotation which are transformed into two series of dephased electric signals by means of photodiodes. Each